Nuclear Engineering and Technology 54 (2022) 3919–3927

Contents lists available at ScienceDirect

Nuclear Engineering and Technology

journal homepage: www.elsevier.com/locate/net

Original Article

Optimization of an extra vessel electromagnetic pump for Lead–Bismuth eutectic coolant circulation in a non-refueling full-life small reactor

Tae Uk Kang [a, 1], Jae Sik Kwak [b, 1], Hee Reyoung Kim [a, *]

[a] Ulsan National Institute of Science and Technology, 50, UNIST-gil, Ulsan, 44919, Republic of Korea
[b] Korea Atomic Energy Research Institute, 111, Daedeok-daero 989 Beon-gil, Yuseong-gu, Daejeon, Republic of Korea

ARTICLE INFO

Article history:
Received 25 September 2020
Received in revised form
19 April 2022
Accepted 30 April 2022
Available online 4 May 2022

Keywords:
LBE
SMR
EVEMP
Electromagnetic pump
Optimization

ABSTRACT

This study presents an optimal design of the coolant system of a non-refueling full-life small reactor by analyzing the space-integrated geometrical and electromagnetic variables of an extra vessel electromagnetic pump (EVEMP) for the circulation of a lead–bismuth eutectic (LBE) coolant. The EVEMP is an ideal alternative to the thermal-hydraulic system of non-refueling full-life micro reactors as it possesses no internal structures, such as impellors or sealing structures, for the transportation of LBE. Typically, the LBE passes through the annular flow channel of a reactor, is cooled by the heat exchanger, and then circulates back to the EVEMP flow channel. This thermal–hydraulic flow method is similar to natural circulation, which enhances thermal efficiency, while providing a golden time for cooling cores in the event of an emergency. When the forced circulation technology of the EVEMP was applied, the non-refueling full-life micro reactor achieve an output power of 60 MWt, which is higher than that achievable via the natural circulation method (30 MWt). Accordingly, an optimized EVEMP for Micro URANUS with a flow rate of 4196 kg/s and developed pressure of 73 kPa under a working temperature of 250 °C was designed.

© 2022 Korean Nuclear Society, Published by Elsevier Korea LLC. This is an open access article under the CC BY-NC-ND license (http://creativecommons.org/licenses/by-nc-nd/4.0/).

1. Introduction

Micro ubiquitous, rugged, accident-forgiving, non-proliferating, and ultra-lasting sustainer (Micro URANUS) is a small module reactor (SMR) with a target output of 60 MWt [1]. Micro URANUS is a pool-type fast reactor with a six-angle grid core that utilizes lead–bismuth eutectic (LBE) as a coolant because of its chemical stability and ability to achieve a fast neutron spectrum. To maintain nuclear non-proliferation, the primary system of the Micro URANUS is designed to function without pumps and for 40 years of operation without the substitution or redeployment of the fuel [2].

To achieve the operation of the reactor without pumps, natural circulation is required not only in accident scenarios but also during common operations. Micro URANUS is a construction that maximizes the natural circulation of LBE by placing a nuclear reactor core, which is a heat source, at the bottom of the reactor vessel, and placing the heat sink (steam generator) at the top. Natural circulation removes heat from the core and transports it to the steam generator, which generates electricity. However, as the size of the power source is significantly smaller than that provided by natural circulation, the pressure drop in the coolant flow area is critical. Table 1 below shows the fundamental dimensions of Micro URANUS reactors, and Fig. 1 shows a comprehensive layout of the reactor.

The potential of an extra vessel electromagnetic pump (EVEMP) to increase the speed of the coolant passing through the eight steam generators of Micro URANUS has been suggested. To achieve this, the pump is installed outside the reactor vessel, in the middle area of the core (Fig. 1). The effectiveness of the electromagnetic pump technology, which is related to EVEMP, in numerous commercial nuclear reactors, such as BN-800, BN-1200, EBR-II, has been verified and designed for gen-IV reactors, such as 4S and PGSFR [3]. For example, electromagnetic pumps for BN-800 have been developed and manufactured as the main pump of the secondary loop and elements of a safety system. These pumps are designed to secure the nominal parameters in the event of an earthquake of magnitude 7 (maximum anticipated earthquake) occurring

* Corresponding author.
E-mail address: kimhr@unist.ac.kr (H.R. Kim).
[1] Kwak and Kang contributed equally to this work.

https://doi.org/10.1016/j.net.2022.04.026
1738-5733/© 2022 Korean Nuclear Society, Published by Elsevier Korea LLC. This is an open access article under the CC BY-NC-ND license (http://creativecommons.org/licenses/by-nc-nd/4.0/).

Table 1
Primary system design specification of Micro URANUS.

Design parameter		Values
Type of steam generator		Double walled
Number of SG		8
Thermal duty/1 HX [MWt]		60/7.5
Steam generator tube length [m]		1.70
Tube-side (LBE)	# of tube	650
	Tube outer diameter [mm]	16.5
	Tube inner diameter [mm]	12.5
	Mass flow (per tube) [kg/s]	0.79
	Core inlet temperature [°C]	250
	Core outlet temperature [°C]	350

simultaneously. Fig. 2 shows a general scheme of a nuclear steam supply system (NSSS) with an electromagnetic pump in a BN-800 reactor [4,5]. In addition, an electromagnetic pump is installed in cold-trap BN-1200 to purify primary sodium. The purification system with cold traps is located in the reactor vessel, which is shown in Fig. 3 [6]. To validate the operation of an electromagnetic pump as a cold trap, various research and development (R&D) activities have been performed. Moreover, sample electro-technical materials for electromagnetic pumps have been subjected to thermal irradiation studies, and mockups of the electromagnetic pumps have been manufactured and tested [6]. As shown in Fig. 4, an electromagnetic pump is used to provide the main flow in the secondary sodium system of EBR II [7]. The main secondary pump is an enclosed, water-cooled, linear-induction electromagnetic pump with a flow rate of 1476 m^3/h and developed pressure of 0.37 MPa [7].

Even under normal operation, a reactor should be monitored to ensure that it is only operated by natural circulation in the event of a pump failure. However, a previous study reported that the current design of reactors only enables an output power of 30 MWt via natural circulation because the transfer of coolant through natural circulation is significantly lower than that of pump use [8].

To enhance the output power of Micro URANUS with very small sizes and specific structures, the installation of EVEMP based on the principle of an electromagnetic pump, which utilizes less space and operates in contactless ways, is required. The target output power of Micro URANUS is 60 MWt, which can be achieved via forced circulation using EVEMP. As the output flow rate under natural circulation (30 MWt) is lower than the target output value (60 MWt), EVEMP was employed in this study to generate additional flowrate to double the output power of the reactor, wherein the heat power is proportional to the flow rate, based on the equation $Q = \dot{m}c\Delta T$ (where Q is the heat power, $\dot{m}$ is the flow rate, c is the specific heat, and T is temperature) [9]. In this study, the EVEMP of Micro URANUS was optimized under the following conditions: flow rate of 4196 kg/s, developed pressure of 73 kPa, and a working temperature of 250 °C.

2. Theoretical approach

In this study, a linear induction electromagnetic pump was designed as the basic model of the EVEMP, and Fig. 5 shows the three-dimensional (3D) view of the pump [10,11]. The pump can be separated into two areas, wherein the first area is a cross-sectional flow channel, which transports the liquid metal exist between the inner and outer pipes. The pipes were composed of SUS 316, which is affected by the reactivity of liquid metals, magnetic flux path distortion, and physical properties [12].

The second area is the electromagnet area, which consists of internal and external cores and coils. This area is composed of high-permeability silicon steel plates and low-electrical resistance copper. A three-phase alternate current was suitably configured in the windings of the copper coils to generate a sinusoidal transverse magnetic field moving in the axial direction. The current travels along the inner core and is induced by the E-shaped teeth section of the outer core of the pump, thus generating in a radius-oriented magnetic field [13]. The LBE flows through the outer working fluid area, and then flows in the opposite direction to the inner working fluid area, after which it circulates in the same way (Fig. 5). In addition, thin layers of silicon steel plates were used as the cores and a lower electrical resistance was used for the coils to reduce the ohmic loss induced by the energy loss of the EVEMP. Thus, the EVEMP was composed of a pump outer core, pump inner core, coils, and flow channel ducts (Fig. 6), was attached to a containment vessel (extra vessel) of Micro URANUS (Fig. 1). The inner core diameter of the pump was fixed at 2500 mm considering the geometry of the reactor core, and the thickness of the inner core of the pump was fixed at 80 mm to sufficiently guide the magnetic flux from the teeth of the pump outer core. As the pump was installed under a steam generator, the maximum pump height was fixed at 2500 mm. The thickness of the flow gap was fixed at 100 mm, and a decrease in this thickness increases the flow velocity, resulting in pressure loss and efficiency problems.

When the three-phase AC current flows from the coil, a time-varying magnetic field was formed along the inner core and outer core of the pump; thus, a current was azimuthally induced in the LBE in the annular cross-sectional duct, where the radial directional magnetic field was formed in the flow channel. Thereby, a Lorentz force was generated from the cross product of the azimuthal current and radial magnetic field.

The Lorentz force, which was obtained using magnetohydrodynamics (MHD) equation, was utilized to perform an MHD analysis based on a fluid equation (continuous equation, kinetic equation). In addition, velocity fields and magnetic fields can be derived by solving the equation. Furthermore, the EVEMP design analysis approach was established through this process, and the results were compared to those of the relationship equation calculated using the electrical equivalent circuit method.

The magnetic field that induced the Lorentz force can be calculated using Maxwell's equation, which is composed of Ampère's law, Faraday's law, and Gauss's law of magnetism, as expressed in Eqs. (1)–(3) [14,15], using ANSYS Maxwell for a coolant channel with a finite length.

$$\text{Ampere}'\text{s law} : \nabla \times \mathbf{H} = \boldsymbol{J} \tag{1}$$

$$\text{Faraday}'\text{s law}: \nabla \times \mathbf{E} = -\frac{\partial \boldsymbol{B}}{\partial t} \tag{2}$$

$$\text{Gauss}'\text{s law for magnetism}: \nabla . \mathbf{B} = 0 \tag{3}$$

The electric field intensity, **E**, induced magnetic field, **B**, and current density from the real coil arrangement, ***J***, exhibit sinusoidal temporal forms, as expressed in Eq. (4).

$$\begin{aligned} E(\mathrm{r},\theta,\mathrm{z}) &= \mathrm{Re}\left[(E_r\hat{r} + E_\theta\hat{\theta} + E_z\hat{z})e^{iwt}\right] \\ B(\mathrm{r},\theta,\mathrm{z}) &= \mathrm{Re}\left[(B_r\hat{r} + B_\theta\hat{\theta} + B_z\hat{z})e^{iwt}\right] \\ \boldsymbol{J}(\mathrm{r},\theta,\mathrm{z}) &= \mathrm{Re}\left[J_\theta e^{iwt}\right]\hat{\theta} \end{aligned} \tag{4}$$

Next, Eq. (1), which is the Ampere's law, was extended using the curls of cylindrical coordinates, as expressed in Eq. (5), and the circumferential component of ***J*** traveling through the coils is expressed in Eq. (6), where μ is the magnetic permeability. The

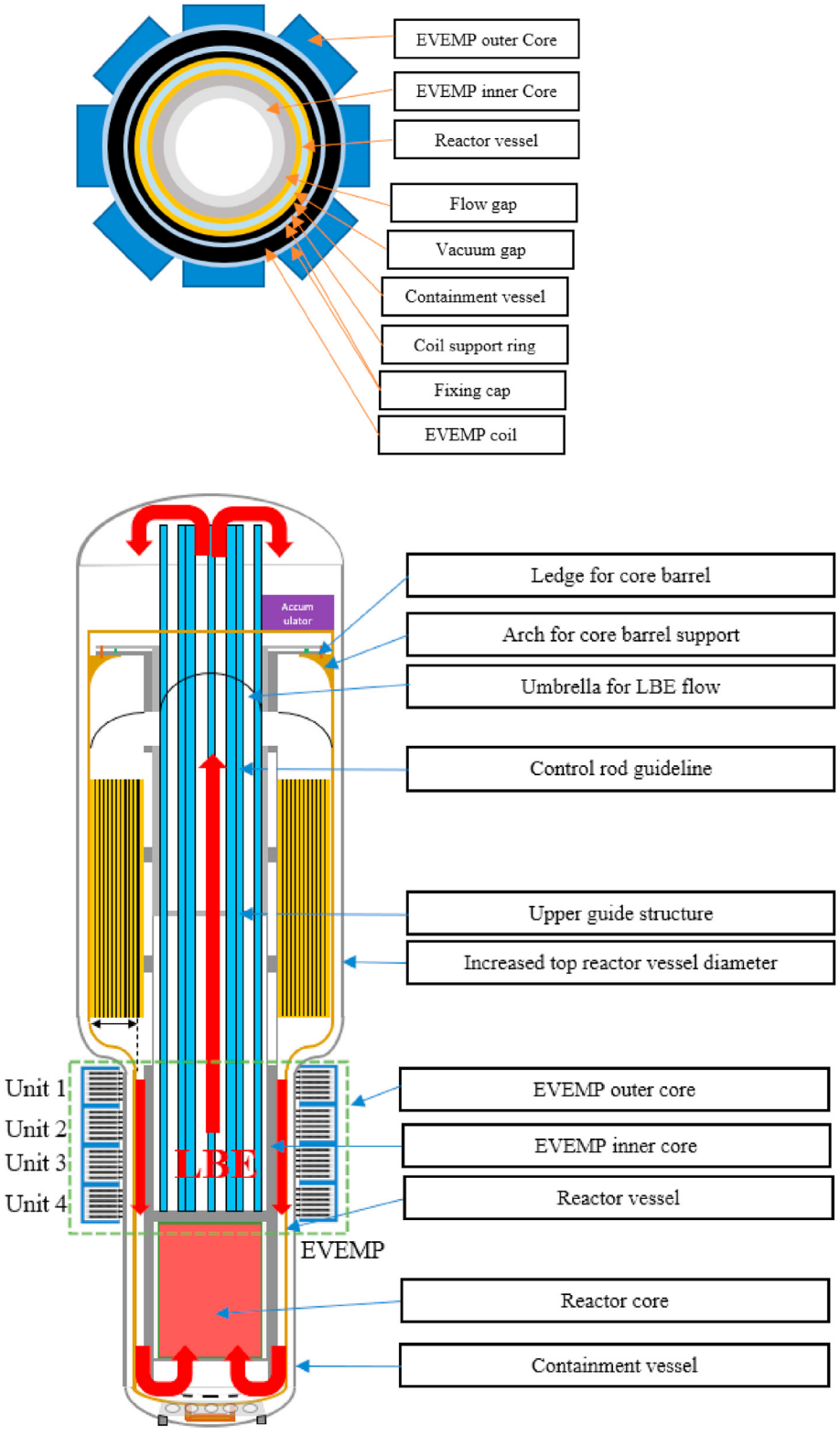

Fig. 1. Schematic of micro ubiquitous, rugged, accident-forgiving, non-proliferating, and ultra-lasting sustainer (Micro URANUS) with extra vessel electromagnetic pump (EVEMP_

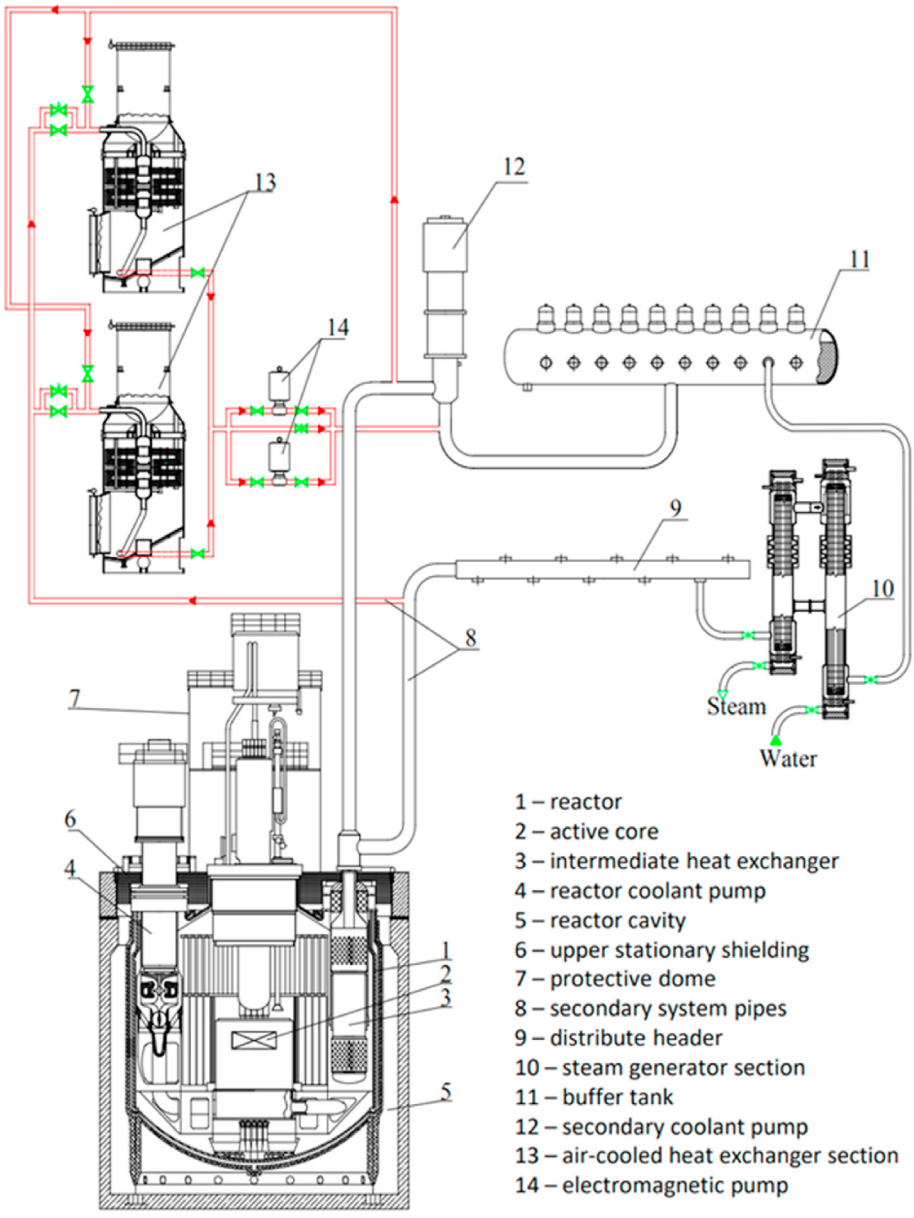

Fig. 2. General scheme of a nuclear steam supply system (NSSS) with BN-800 reactor.

radial and axial components have been deleted in Eqs. (5) and (6), which may then be combined to obtain Eq. (7) [16].

$$\nabla \times \mathbf{B} = Re\left[e^{iwt}\right]\Bigg[\times \left(\frac{1}{r}\frac{\partial B_z}{\partial \theta} - \frac{\partial B_\theta}{\partial z}\right)\widehat{r} + \left(\frac{\partial B_r}{\partial z} - \frac{\partial B_z}{\partial r}\right)\widehat{\theta} + \frac{1}{r}\left(\frac{\partial (rB_z)}{\partial r} - \frac{\partial B_r}{\partial \theta}\right)\widehat{z}\Bigg] \quad (5)$$

$$\mu \boldsymbol{J} = \mu \mathrm{Re}\left[J_\theta e^{iwt}\right]\widehat{\theta} \quad (6)$$

$$\mu J_\theta = \frac{\partial B_r}{\partial z} - \frac{\partial B_z}{\partial r} \quad (7)$$

Similarly, the left side of Eq. (2) can be expanded to obtain Eq. (8), and the magnetic field can be separated into radial, circumferential, and axial components, as expressed in Eq (9). Considering the axial symmetry, Eqs. (8) and (9) can be combined to form Eq. (10), and Eq. (11) can be obtained by arranging Eq. (10) according to the component (11).

$$\nabla \times \mathbf{E} = Re\left[e^{iwt}\right]\Bigg[\times \left(\frac{1}{r}\frac{\partial E_z}{\partial \theta} - \frac{\partial E_\theta}{\partial z}\right)\widehat{r} + \left(\frac{\partial E_r}{\partial z} - \frac{\partial E_z}{\partial r}\right)\widehat{\theta} + \frac{1}{r}\left(E_z + r\frac{\partial E_z}{\partial r} - \frac{\partial E_r}{\partial \theta}\right)\widehat{z}\Bigg] \quad (8)$$

$$-\frac{\partial \boldsymbol{B}}{\partial t} = -iw(B_r\widehat{r} + B_\theta\widehat{\theta} + B_z\widehat{z})Re\left[e^{iwt}\right] \quad (9)$$

$$\left(-\frac{\partial E_\theta}{\partial z}\right)\widehat{r} + \left(\frac{\partial E_r}{\partial z} - \frac{\partial E_z}{\partial r}\right)\widehat{\theta} + \frac{1}{r}\left(E_z + r\frac{\partial E_z}{\partial r}\right)\widehat{z} = -iw(B_r\widehat{r} + B_\theta\widehat{\theta} + B_z\widehat{z}) \quad (10)$$

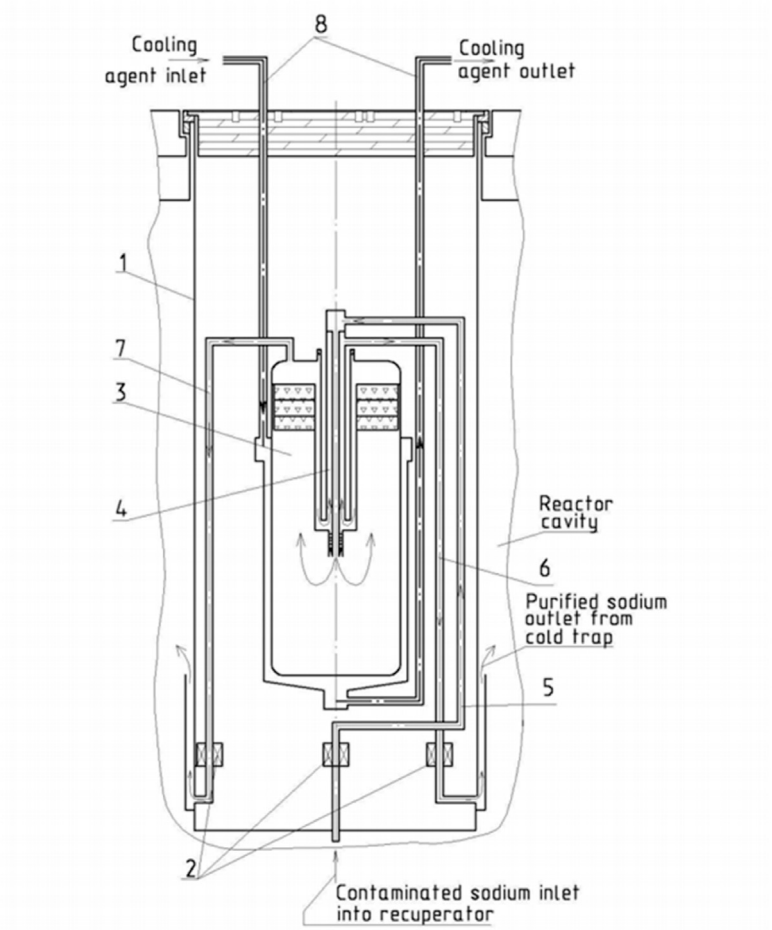

1 - casing of built-up cold trap; 2 – electromagnetic devices; 3 - working cavity of cold trap; 4 – recuperator; 5 - pipeline of contaminated sodium supply to recuperator; 6 - pipeline of purified sodium discharge from recuperator; 7 - pipeline of purified sodium bypass from working cavity; 8 - pipelines of cooling agent supply and discharge

Fig. 3. Schematic of the BN-1200 cold trap.

$$\frac{\partial E_\theta}{\partial z} = iwB_r, \quad \frac{\partial E_r}{\partial z} - \frac{\partial E_z}{\partial r} = -iwB_\theta, \quad \frac{1}{r}\left(E_z + r\frac{\partial E_z}{\partial r}\right) = -iwB_z \tag{11}$$

The electric field generated in the channel can be expressed as Eq. (12) by substituting Eq. (11) into Eq. (7), which contains the circumferential component of Ampere's equation, and omitting the magnetic field component.

$$\begin{aligned}\mu J_\theta &= \frac{\partial B_r}{\partial z} - \frac{\partial B_z}{\partial r} = \frac{1}{iw}\left(\frac{\partial^2 E_\theta}{\partial z^2} + \frac{\partial\left(\frac{1}{r}\left(E_z + r\frac{\partial E_z}{\partial r}\right)\right)}{\partial r}\right) \\ &= \frac{1}{iw}\left(\frac{\partial^2 E_\theta}{\partial z^2} - \frac{1}{r^2}E_z + \frac{1}{r}\frac{\partial E_z}{\partial r} + \frac{\partial^2 E_z}{\partial r^2}\right)\end{aligned} \tag{12}$$

With each component of the magnetic field in cylindrical dimensions and axial symmetry, Gauss's equation of magnetism in Eq. (3) can be represented as Eq. (13)

$$\frac{1}{r}\left(B_r + r\frac{\partial B_r}{\partial r}\right) + \frac{\partial B_z}{\partial z} = 0 \tag{13}$$

Accordingly, Eqs. (7) and (13) can be combined to obtain Eqs. (14) and (15), which are the radial and axial components of the magnetic field.

$$\frac{\partial}{\partial r}\frac{1}{r}\left(B_r + r\frac{\partial B_r}{\partial r}\right) + \frac{\partial^2 B_r}{\partial z^2} = \mu\frac{\partial J_\theta}{\partial z} \tag{14}$$

$$\frac{1}{r}\frac{\partial B_z}{\partial r} + \frac{\partial^2 B_z}{\partial r^2} + \frac{\partial^2 B_z}{\partial z^2} = -\mu\left(\frac{1}{r}J_\theta + \frac{\partial J_\theta}{\partial r}\right) \tag{15}$$

Based on the EVEMP 3D modelling using ANSYS Maxwell and ANSYS Fluent, a numerical study of the EVEMP design parameters was performed, wherein the velocity at the wall boundary of the annular flow channel is constant.

The Navier–Stokes equation is a non-linear partial differential equation, and its solution provides data on velocity or flow fields, which define the velocity of a fluid at a specific position in space and time. Other quantities, such as flow rate can be determined after solving the velocity field. When the Navier–Stokes equation is stated in the cylindrical coordinates system r, θ, z, the system of Eq. (16–18) is produced, where ρ is the density, η is the dynamic viscosity, and V is the volume.

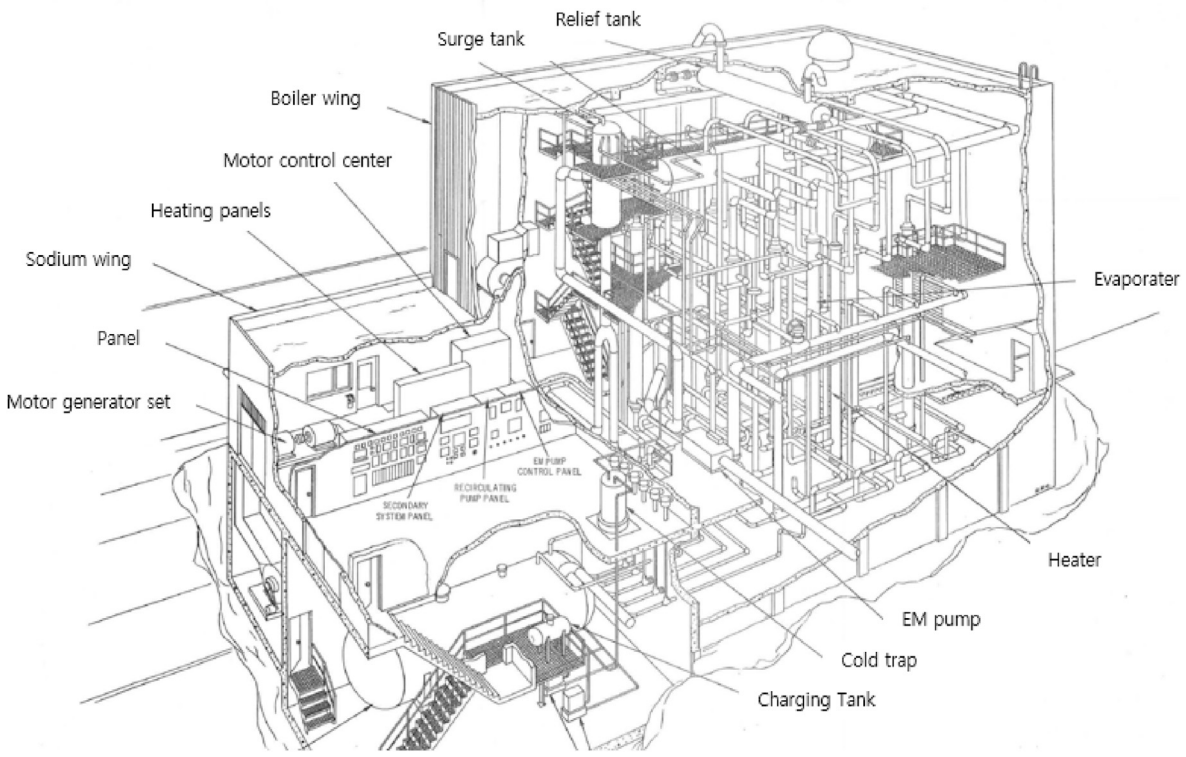

Fig. 4. EBR II piping system.

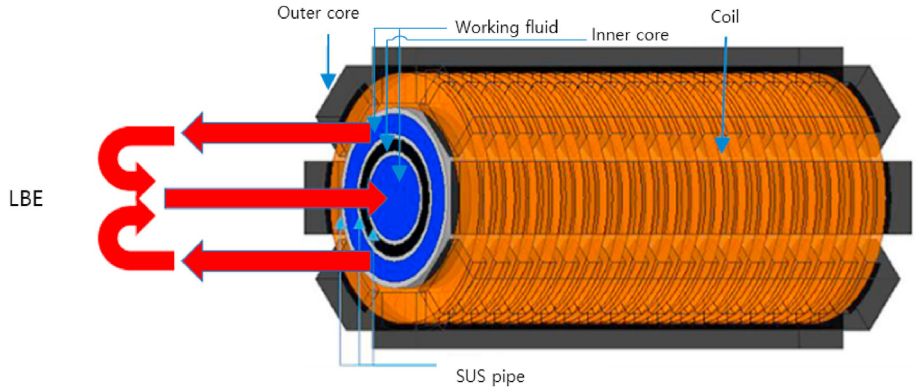

Fig. 5. General structures of the EVEMP.

$$\rho\left(\frac{\partial v_r}{\partial t}+v_r\frac{\partial v_r}{\partial r}+\frac{v_\theta}{r}\frac{\partial v_r}{\partial \theta}+v_z\frac{\partial v_r}{\partial z}-\frac{v_\theta}{r}\right)=-\frac{\partial p}{\partial r}+\eta\left[\frac{1}{r}\frac{\partial}{\partial r}\left(r\frac{\partial v_r}{\partial r}\right)+\frac{1}{r^2}\frac{\partial^2 v_r}{\partial \theta^2}+\frac{\partial^2 v_r}{\partial z^2}-\frac{v_r}{r^2}-\frac{2}{r^2}\frac{\partial v_\theta}{\partial \theta}\right]+\frac{f_r}{V} \tag{16}$$

$$\rho\left(\frac{\partial v_\theta}{\partial t}+v_r\frac{\partial v_\theta}{\partial r}+\frac{v_\theta}{r}\frac{\partial v_\theta}{\partial \theta}+v_z\frac{\partial v_\theta}{\partial z}-\frac{v_r v_\theta}{r}\right)=-\frac{1}{r}\frac{\partial p}{\partial \theta}+\eta\left[\frac{1}{r}\frac{\partial}{\partial r}\left(r\frac{\partial v_\theta}{\partial r}\right)+\frac{1}{r^2}\frac{\partial^2 v_\theta}{\partial \theta^2}+\frac{\partial^2 v_\theta}{\partial z^2}+\frac{v_\theta}{r^2}+\frac{2}{r^2}\frac{\partial v_r}{\partial \theta}\right]+\frac{f_\theta}{V} \tag{17}$$

$$\rho\left(\frac{\partial v_z}{\partial t}+v_r\frac{\partial v_z}{\partial r}+\frac{v_\theta}{r}\frac{\partial v_z}{\partial \theta}+v_z\frac{\partial v_z}{\partial z}\right)=-\frac{\partial p}{\partial z}+\eta\left[\frac{1}{r}\frac{\partial}{\partial r}\left(r\frac{\partial v_z}{\partial r}\right)+\frac{1}{r^2}\frac{\partial^2 v_z}{\partial \theta^2}+\frac{\partial^2 v_z}{\partial z^2}\right]+\frac{f_z}{V} \tag{18}$$

The Lorentz force (electromagnetic force) of the EVEMP, which is axially (z-direction) produced in the flow channel from the cross product of the azimuthal current and radial magnetic field, is expressed in Eq. (19). In the Navier–Stokes equation, the force density calculated using Eq. (19) was used as the source term, where σ is the electrical conductivity

$$\mathbf{f}=\mathbf{J}\times\boldsymbol{B}=\left(\sigma E_\theta B_r-\sigma v_z {B_r}^2\right)\hat{z} \tag{19}$$

where. $\mathbf{J}=\sigma(\mathbf{E}+\mathbf{v}\times\mathbf{B})$

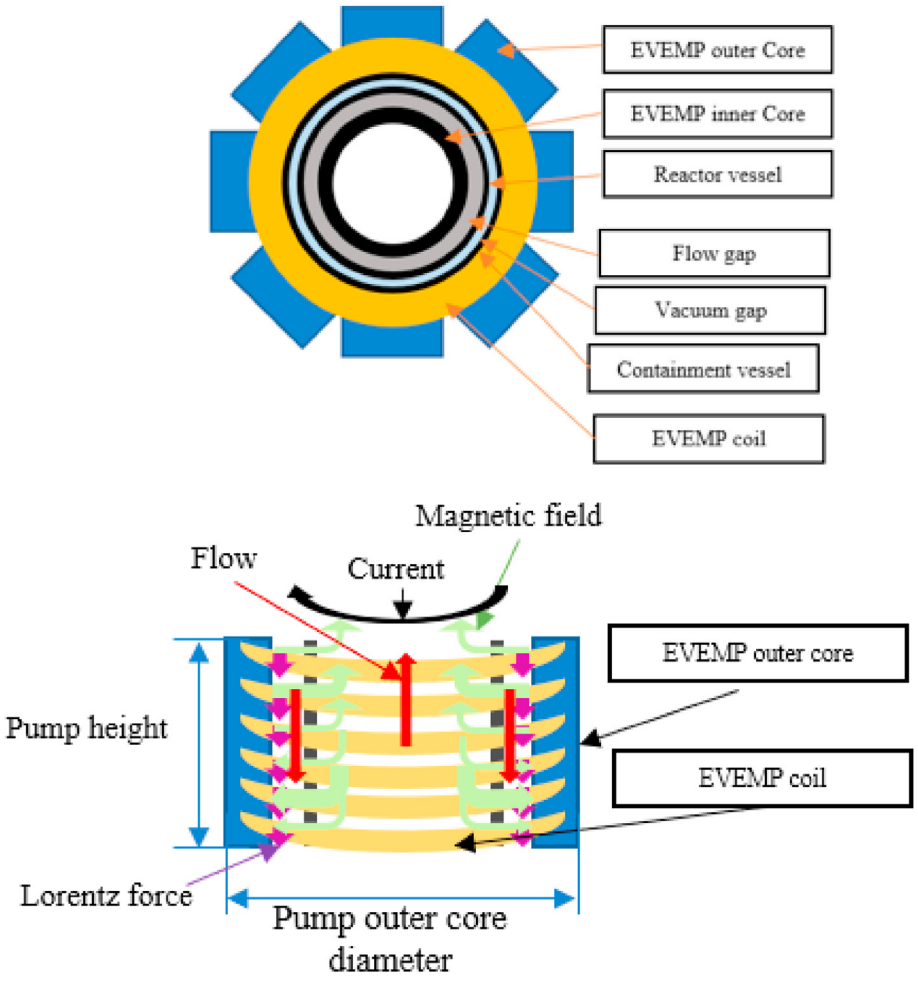

Fig. 6. Operation of the EVEMP in the Micro URANUS (one pump unit basis).

3. Results and discussion

The effects and performance of EVEMP in the Micro URANUS with changes in the geometrical variables and electromagnetic variables were analyzed [17]. The main design variables of EVEMP include geometrical variables, such as pump outer core diameter and pump inner core thickness, and electromagnetic variables, such as pole pairs and frequency. The performance of the EVEMP correlated with the design variables (Figs. 7–10).

The frequency of the input power affected the performance of EVEMP in two ways: skin depth and slip. Skin depth or skin effect corresponds to the point where the current density was the largest near the surface of the conductor. A change in the electromagnetic field induced eddy currents near the surface, and skin depth is defined as the thickness layer where 87% of the power is generated, according to Eq. (20) where f = frequency [Hz], σ = conductivity [S/m], and μ = permeability [H/m].

$$\delta = \frac{1}{\sqrt{\pi f \sigma \mu}} \tag{20}$$

This indicates that at the same thickness, a high frequency, conductivity, and permeability resulted in tremendous energy loss (Table 2). Because the thicknesses of the flow gap, and inner and outer ducts were higher than that of the general electromagnetic pump, the loss caused by skin effect is important. The slip corresponds to the ratio of difference between the synchronous velocity and flow velocity, as expressed in Eq. (21) where V_s = synchronous velocity, V_f = velocity of fluid, s = slip. Because the developed pressure and slip can be expressed using Eq. (22) where I = current, Q = flow rate, R_2 = secondary resistance, X_m = magnetic reactance, it is essential to determine the appropriate slip value from the optimization process.

$$s = \frac{V_s - V_f}{V_s} \tag{21}$$

$$P = \frac{3I^2}{Q} \frac{R_2(1-s)}{s\left(\frac{R_2{}^2}{X_m s^2} + 1\right)} \tag{22}$$

The developed pressure and efficiency of the EVEMP were optimized on a specified range of pole pitch, which can be expressed using Eq. (23), where L = Pump height, p = the number of pole pairs, and τ = pole pitch.

$$L = 2p\tau \tag{23}$$

Figs. 7 and 8 show the graphs of the developed pressure and efficiency with a change in the number of pole pairs and pump outer core diameter, which were interpreted at 5 and 10 Hz. To reduce the end effect of the electromagnetic pump, a low input frequency was utilized [18]. The efficiency and developed value increased and then decreased beyond a certain point with an

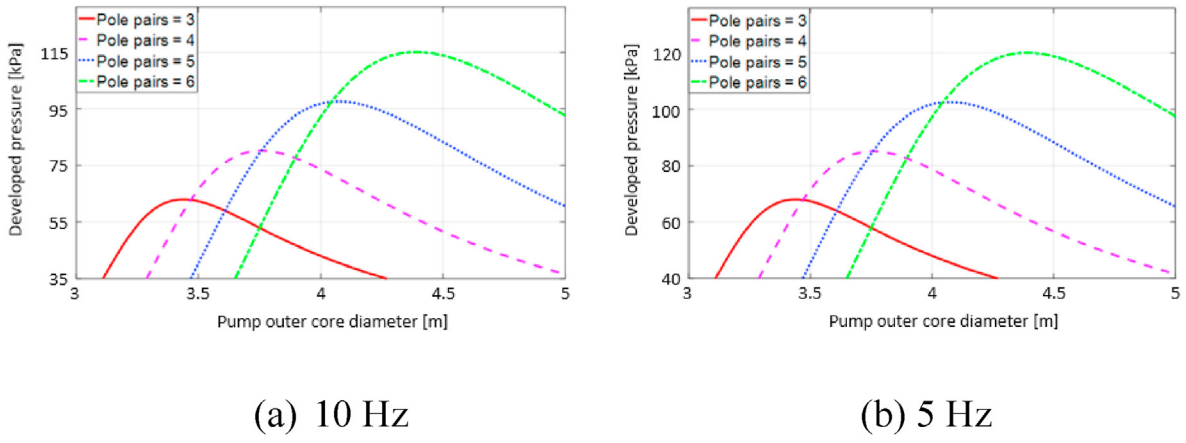

Fig. 7. Developed pressure of the EVEMP with a change in the pump outer core diameter at different number of pole pairs ((a) f = 10 Hz, (b) f = 5 Hz).

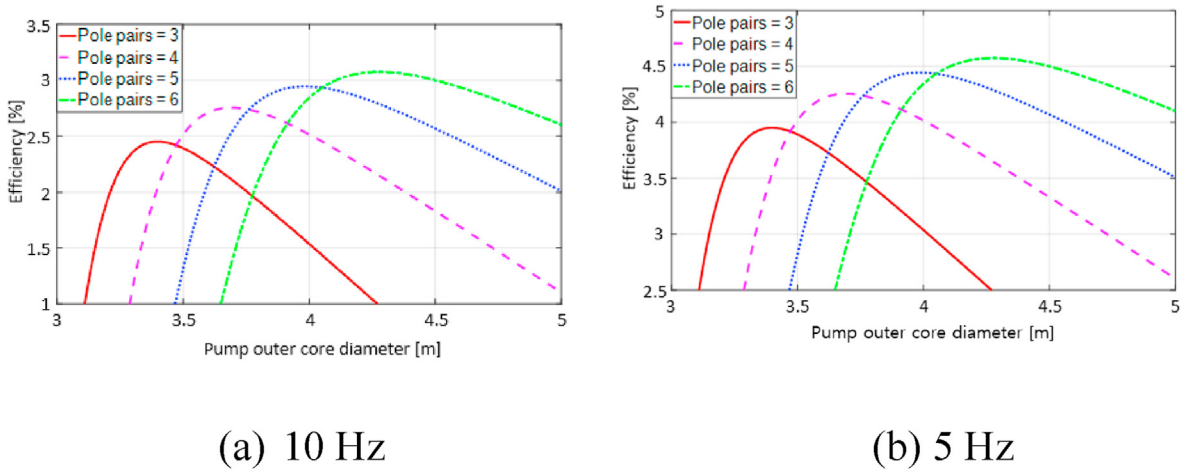

Fig. 8. Efficiency of the EVEMP with a change in the pump outer core diameter at different number of pole pairs ((a) f = 10 Hz, (b) f = 5 Hz).

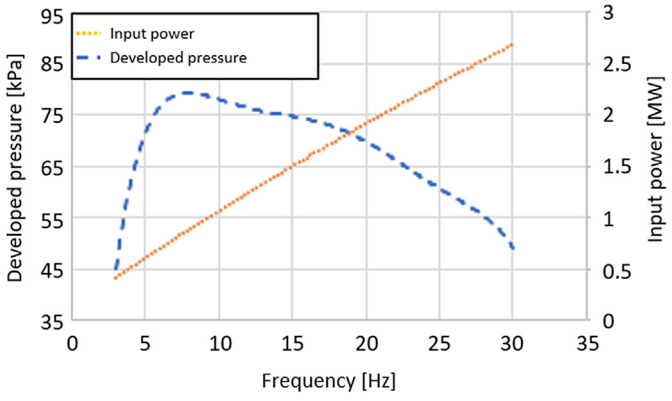

Fig. 9. Input power and developed pressure of the EVEMP as a function of frequency.

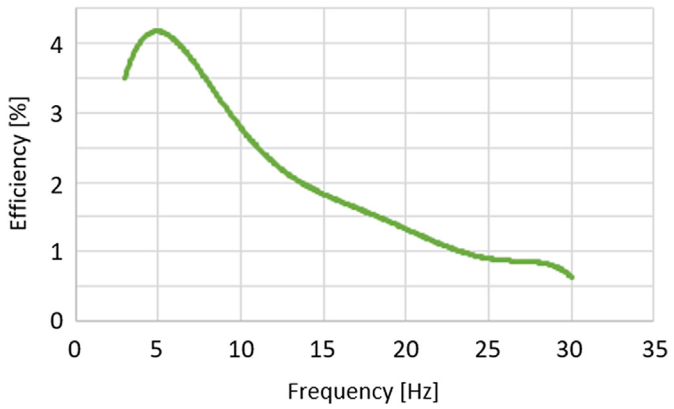

Fig. 10. Efficiency of EVEMP as a function of frequency.

increase in the pump outer core diameter. When the diameter was too short, the induced magnetic field was not smooth owing to a decrease in the tooth section. When the diameter was too large, the resistance increased, resulting in ohmic loss. Therefore, it is essential to determine the optimum diameter, and the optimum values in both graphs were between 3600 and 3700 mm. Therefore, considering the coil thickness and reactor size, the optimum pump outer core diameter was determined 3683 mm. In addition, the efficiency and developed pressure values in both graphs increased with an increase in the number of pole pairs. However, the maximum pump height was limited to 2500 mm because the EVEMP was located between the steam generator and the core. This indicates that a maximum of four pole pair can be used because the height of the pump corresponding to one pole pair was 544.6 mm.

Table 2
Skin depth of various materials as a function of frequency.

Frequency [Hz]	Steel AISI 316 ($\mu_r = 1$) [mm]	Copper ($\mu_r \cong 1$) [mm]	Steel AISI 420 ($\mu_r =$ 2000) [mm]	LBE ($\mu_r \cong 1$) [mm]
60	55.9	8.62	1.07	27.24
100	43.32	6.68	0.83	21.1
1000	13.70	2.11	0.26	6.67
10,000	4.33	0.67	0.08	2.12
100,000	1.37	0.21	0.026	0.664
200,000	0.97	0.15	0.019	0.474
1,000,000	0.43	0.067	0.008	0.212

Table 3
Design specifications of EVEMP.

	Design variables	Unit	Values
Requirements	Mass flow	[kg/s]	4196
	Developed pressure	[kPa]	73
	Temperature	[°C]	250
	Velocity	[m/s]	0.512
Geometrical	Pump height	[mm]	2178
	Pump outer core diameter	[mm]	3683
	Pump inner core diameter	[mm]	2500
	Pump outer core thickness	[mm]	566.5
	Pump inner core thickness	[mm]	80
	Flow gap	[mm]	100
Electrical	Input current	[A]	1250
	Input voltage	[V]	875
	Input VI	[kVA]	1894
	Input power	[kW]	675
	Frequency	[Hz]	5
	Efficiency	[%]	4.15

Figs. 9 and 10 show the developed pressure and input power of the EVEMP with a change in the frequency under the following conditions: pump outer core diameter of 3683 mm, four pole pairs, and input current of 1250 A. The pump specification increases as the input current increases; however, based on the maximum allowable current of the coil, a maximum current of 1250 A was recommended, and was adopted as the current. The input power increased with an increase in the frequency because higher frequency results in a low electric conductivity in the flow owing to the skin effect (Fig. 9). The optimum developed pressure value was achieved at a frequency of approximately 8 Hz. Although the optimum developed pressure was achieved at approximately 8 Hz, the optimum efficiency was achieved at approximately 5 Hz (Fig. 10), which is because the efficiency corresponded to the ratio of the hydraulic power ($\Delta P \bullet Q$) to input power. With an increase in the frequency to 5 Hz, the increase in the developed pressure value was large, thus the efficiency increased; however, with a further increase in the frequency beyond 5 Hz, the increase in the developed pressure value decreased, thus decreasing the efficiency. These results indicate that the optimal frequency (5 Hz), input voltage (875 V), and input power (675 kW) of the pump were achieved at 1250 A. The optimized design specifications of EVEMP are listed in Table 3.

4. Conclusion

In this study, an EVEMP with a mass flow of 4196 kg/s and a developed pressure of 73 kPa at an operating temperature of 250 °C was optimally designed. The results demonstrated that the EVEMP exhibited optimal pump outer core diameter and pump height geometrically, and the optimal input frequency and pole pairs electromagnetically at an input power of 675 kW. The optimized EVEMP is expected to be used suitably to satisfy the required thermal output (60 MWt) of Micro URANUS.

Declaration of competing interest

The authors declare that they have no known competing financial interests or personal relationships that could have appeared to influence the work reported in this paper.

Acknowledgements

This research was supported by the National Nuclear R&D program funded by the Ministry of Science and ICT and by the National Nuclear R&D program (NRF-2019M2D1A1067205).

References

[1] S.M. Kim, J.H. Cho, I.S. Hwang, The Development of LBE Integral Test Loop, HELIOS and Tests by Using HELIOS, Transactions of the Korean Nuclear Society Autumn Meeting, 2011.
[2] H.R. Kim, Y.B. Lee, A design and characteristic experiment of the small annular linear induction electromagnetic pump, Ann. Nucl. Energy 38 (5) (2011) 1046–1052.
[3] Y. Nishi, N. Ueda, I. Kinoshita, T. Koga, S. Nishimura, T. Yokoyama, S. Kasai, A new concept of the 4S reactor and thermal hydraulic characteristics, Proc. Int. Conf. Nucl. Eng. 46873 (2004) 385–394. January.
[4] Ilia Pakhomov, BN-600 AND BN-800 OPERATING EXPERIENCE, Presentation in SSC RF-IPPE, Russia, 2018. December 19.
[5] A.M. Anisimov, I.V. Vitkovsky, M.M. Golovanov, I.R. Kirillov, Electromagnetic pumps for BN-800, At. Energy 112 (6) (2012) 443.
[6] V.T. Berikbosinov, D.V. Gusev, A.E. Komarov, S.A. Rogozhkin, S.V. Rukhlin, S.F. Shepelev, A.A. Shumsky, Development of the Built-In Primary Sodium Purification System for the Advanced BN-1200 Reactor Plant, 2017.
[7] C.W. Grandy, Trade study of IHTS EM pump placement DRAFT, in: Presentation in PGSFR Meeting, Republic of Korea, 2015. March 5.
[8] T.D.C. Nguyen, M.F. Khandaq, E. Jeong, J. Choe, D. Lee, D.A. Fynan, Micro-URANUS, Core design for long-cycle lead-bismuth-cooled fast reactor for marine applications, Int. J. Energy Res. 45 (8) (2021) 12426–12448.
[9] B. Awad, M. Chaudry, J. Wu, N. Jenkins, Integrated optimal power flow for electric power and heat in a microgrid, in: CIRED 2009-20th International Conference and Exhibition on Electricity Distribution-Part 1, IET, June, 2009, pp. 1–4.
[10] J. Kwak, H.R. Kim, Design optimization analysis of a large electromagnetic pump for sodium coolant transportation in PGSFR, Ann. Nucl. Energy 121 (2018) 62–67.
[11] K. Aizawa, Y. Chikazawa, S. Kotake, K. Ara, R. Aizawa, H. Ota, Electromagnetic pumps for main cooling systems of commercialized sodium-cooled fast reactor, J. Nucl. Sci. Technol. 48 (3) (2011) 344–352.
[12] K. Bessho, S. Yamada, M. Nakano, K. Nakamoto, A new flux concentration type electromagnetic pump for FBR, J. Magn. Magn Mater. 112 (1–3) (1992) 419–422.
[13] M. Ishii, I. Kataoka, Scaling laws for thermal-hydraulic system under single phase and two-phase natural circulation, Nucl. Eng. Des. 81 (3) (1984) 411–425.
[14] H.R. Kim, J.S. Kwak, MHD design analysis of an annular linear induction electromagnetic pump for SFR thermal hydraulic experimental loop, Ann. Nucl. Energy 92 (2016) 127–135, 2016.
[15] S.A. Nasar, I. Boldea, Linear Motion Electric Machines, John Wiley & Sons, 1976.
[16] J. Kwak, H.R. Kim, Magnetic field analysis of an electromagnetic pump for sodium thermohydraulic test in the sodium test loop for safety simulation and assessment—phase 1, Prog. Nucl. Energy 101 (2017) 235–242.
[17] J. Kwak, H.R. Kim, Development of innovative reactor-integrated coolant system design concept for a small modular lead fast reactor, Int. J. Energy Res. 42 (13) (2018) 4197–4205.
[18] H.R. Kim, J.S. Kwak, MHD design analysis of an annular linear induction electromagnetic pump for SFR thermal hydraulic experimental loop, Ann. Nucl. Energy 92 (2016) 127–135.